Adjoint High-Order Vectorial Finite Elements for Nonsymmetric Transversally Anisotropic Waveguides

Volkmar Schulz

***Abstract*—In this paper, a vector finite-element method (FEM) for the investigation of microwave and optical waveguides with arbitrary cross section is presented. In particular, the FEM solves the vector wave equation in the frequency domain for waveguides, containing nonsymmetric transversally anisotropic (passive and active) materials. Therefore, a bilinear form has been derived that is solved for the original and adjoint wave equation. Bi-orthogonality, relations of original and adjoint solutions for simpler materials, the role of nonphysical solutions for both problems, and their proper approximations are discussed in detail. Special focus has been set on shifting the propagation constants of the nonphysical modes for nonzero frequencies to infinity. Therefore, an excellent rate of convergence for iterative solvers is observed. The occurrence of nonphysical solutions is shown. Different nth-order basis functions are systematically derived, which are identical to the well-known tangential continuous finite elements. Both algebraic eigenvalue problems are solved via a generalized Lanczos algorithm, which solves both eigenvalue problems efficiently. The capability of the FEM is illustrated by critical examples.**

***Index Terms*—Adjoint, anisotropic, bi-orthogonality, finite-element method (FEM), Lanczos, microstrip, nonphysical, nonsymmetric, optical, spurious, tangential continuous, transversal, vectorial wave equation, waveguide.**

I. Introduction

THE increasing complexity of microwave and optical components requires accurate numerical tools to predict waveguide parameters qualitatively and quantitatively. Today, many numerical methods are known, which are able to handle different types of waveguide problems. Especially for microwave structures, numerical methods have to be able to handle fields at sharp edges [1], [2]. For optical components, very accurate predictions of fields and propagation constants are needed. Since the optimization of waveguide components increases the complexity of the cross sections and the applied material systems, the finite-element method (FEM) represents one of the most suitable methods for future investigations.

However, solving the vectorial wave equation with numerical methods often leads to the occurrence of nonphysical or spurious solutions. Unfortunately, first ideas of forcing the field to be source-free by penalty methods only partially succeed [3]. Other authors successfully used formulations only in the transversal field components [4]. Over the last ten years, several papers have been published, in which tangential continuous finite elements (TCFEs) successfully suppressed these nonphysical solutions [5]–[8]. An additional advantage of these TCFEs is the possibility to handle fields at sharp perfect conductive or dielectric edges [9]. These two features prepare the TCFE for the analysis of all microstrip-like waveguides.

Most of the TCFE-based FEMs are limited to lossless or complex, but symmetric transversally anisotropic materials [7], [10]–[12]. In [13], a TCFE-based FEM is derived, which is able to handle general lossy anisotropic media by increasing the dimension of the algebraic eigenvalue problem. In this paper, a generalized bilinear form will be derived, which is able to investigate waveguides with arbitrarily complex (passive or active) nonsymmetric transversally anisotropic materials. Therefore, unlike other authors, the original and adjoint problem is solved to generate a set of bi-orthogonal functions.

Different high-order TCFEs have been published [7], [11]–[15]. Thus, this paper tries to improve the understanding of the occurrence and the avoidance of nonphysical solutions. In contrast to other authors [5], [8], [10], [15], [17], the finite-element (FE) function space of nth order will be directly derived from the bilinear form itself. It will be shown that, in case of unsuited basis functions, a nonphysical solution will pollute the eigenvalue spectrum. A special focus will be set to derive a bilinear form, in which all nonphysical solutions for nonzero frequency appear at infinity. Important relations between the physical, adjoint, and nonphysical solutions will be deduced. The algebraic eigenvalue of the original and adjoint problem will be obtained by using a generalized Lanczos algorithm [5] and a sparse LU decomposition [16]. Excellent rate of convergence is observed, even for calculations at or close to cutoff frequencies.

II. Formulation

A. Governing Equations

We consider a passive or active anisotropic nonsymmetric microwave or optical waveguide with arbitrary limited cross section Ω (see Fig. 1). $\partial\Omega\,(=\partial\Omega_D \cup \partial\Omega_N)$ is the boundary of the region Ω. For the investigation of waveguides, the dependency of the field quantities on the time t and the axial coordinate z is assumed to be of the following form:

$$\boldsymbol{\mathcal{F}}(x,y,z,t) = \boldsymbol{F}(x,y)e^{j\omega t-\gamma z}. \tag{1}$$

$\gamma = \alpha + j\beta$ denotes the propagation constant with the attenuation α and the phase constant β. The propagation of electromagnetic energy in the z-direction is described by the two linear independent Maxwell's equations

$$\beta_0 \neq 0\text{: } (\boldsymbol{\nabla}_t - \boldsymbol{z}_0\gamma) \times \boldsymbol{E} = -\,j\beta_0 Z_0 \boldsymbol{\mu}_r \boldsymbol{H} \tag{2a}$$

Manuscript received April 10, 2002; revised November 19, 2002.

The author is with the Philips Research Laboratories of Hamburg, D-22335 Hamburg, Germany (e-mail: volkmar.schulz@web.de).

Digital Object Identifier 10.1109/TMTT.2003.809673

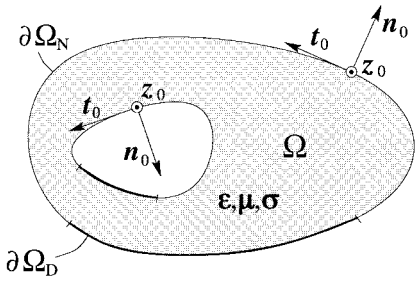

Fig. 1. Waveguide with arbitrary cross section.

$$(\nabla_t - \boldsymbol{z}_0\gamma) \times \boldsymbol{H} = \jmath\frac{\beta_0}{Z_0}\boldsymbol{\varepsilon}_r\boldsymbol{E}. \tag{2b}$$

Here, $\nabla_t = \boldsymbol{x}_0(\partial/\partial x) + \boldsymbol{y}_0(\partial/\partial y)$ is the transversal Nabla operator and $\boldsymbol{\varepsilon}_r$ and $\boldsymbol{\mu}_r$ are the relative permittivity and permeability tensors with complex entries. $\boldsymbol{x}_0$, $\boldsymbol{y}_0$, and $\boldsymbol{z}_0$ are the unit vectors along the x-, y-, and z-axis. $\beta_0 = \omega\sqrt{\varepsilon_0\mu_0}$ denotes the free-space wavenumber, ω is the angular frequency, and $Z_0 = \sqrt{\mu_0/\varepsilon_0}$ is the free-space wave impedance. The scalar quantities ε_0 and μ_0 are the permittivity and permeability of vacuum, respectively. For unique solutions of (2), the following boundary conditions are assumed:

$$\boldsymbol{n}_0 \times \boldsymbol{E} = \boldsymbol{0}, \qquad \text{on } \partial\Omega_D \tag{3a}$$

$$\boldsymbol{n}_0 \times \boldsymbol{H} = \boldsymbol{0}, \qquad \text{on } \partial\Omega_N. \tag{3b}$$

Here, $\boldsymbol{n}_0$ is the unit vector perpendicular to the boundary $\partial\Omega$, pointing outside the region Ω.

All materials are transversally anisotropic quantities, e.g.,

$$\boldsymbol{\mu}_r = \begin{bmatrix} \boldsymbol{\mu}_{tt} & 0 \\ 0 & \mu_{zz} \end{bmatrix} \quad \boldsymbol{\mu}_{tt} = \begin{bmatrix} \mu_{xx} & \mu_{xy} \\ \mu_{yx} & \mu_{yy} \end{bmatrix}. \tag{4}$$

No additional restrictions have been made for the materials so neither hermitic ($\boldsymbol{\mu}_r = \boldsymbol{\mu}_r^H$, $\boldsymbol{\varepsilon}_r = \boldsymbol{\varepsilon}_r^H$), nor symmetric ($\boldsymbol{\mu}_r = \boldsymbol{\mu}_r^T$, $\boldsymbol{\varepsilon}_r = \boldsymbol{\varepsilon}_r^T$) materials have been imposed. Waveguides containing transversally anisotropic conductivity $\boldsymbol{\sigma}$ can be investigated via

$$\boldsymbol{\varepsilon}_r = \boldsymbol{\epsilon}_r - \jmath\frac{\boldsymbol{\sigma}}{\omega\varepsilon_0}. \tag{5}$$

Here, $\boldsymbol{\epsilon}_r$ denotes the previous permittivity tensor. Transversally anisotropic materials are also known as reflection-symmetric materials because $\pm\gamma$ are valid propagation constants [20]. Furthermore, from (2a) and (2b), second-order vectorial wave equations for either the electric or magnetic field can be deduced. Without any restriction, a formulation based on the electric field is used

$$\beta_0^2\boldsymbol{\varepsilon}_r\boldsymbol{E} = (\nabla_t - \boldsymbol{z}_0\gamma) \times \mu_r^{-1}\left[(\nabla_t - \boldsymbol{z}_0\gamma) \times \boldsymbol{E}\right]. \tag{6}$$

A formulation in the magnetic field is simply achieved by exchanging the quantities $\boldsymbol{E}$, $\boldsymbol{\varepsilon}_r$, and $\boldsymbol{\mu}_r^{-1}$ with $\boldsymbol{H}$, $\boldsymbol{\mu}_r$, and $\boldsymbol{\varepsilon}_r^{-1}$. Instead of using $\boldsymbol{\mu}_r^{-1}$, the rearranged definition

$$\boldsymbol{\eta}_{tt} = \frac{\begin{bmatrix} \mu_{xx} & \mu_{yx} \\ \mu_{xy} & \mu_{yy} \end{bmatrix}}{\mu_{xx}\mu_{yy} - \mu_{xy}\mu_{yy}} \quad \eta_{zz} = \frac{1}{\mu_{zz}} \tag{7}$$

is used to simplify the notation [14]. Thus, the vector wave equation is separated into a transversal and longitudinal part

$$\nabla_t \times \eta_{zz}(\nabla_t \times \boldsymbol{E}_t) - \gamma\boldsymbol{\eta}_{tt}(\nabla_t E_z + \gamma\boldsymbol{E}_t) = \beta_0^2\boldsymbol{\varepsilon}_{tt}\boldsymbol{E}_t \tag{8a}$$

$$-\nabla_t \cdot \boldsymbol{\eta}_{tt}(\nabla_t E_z + \gamma\boldsymbol{E}_t) = \beta_0^2\varepsilon_{zz}E_z. \tag{8b}$$

For a typical calculation, the frequency is known, whereas γ^2 is the demanded eigenvalue. Thus, it is useful to transform (6) with

$$\gamma \neq 0\text{: } \boldsymbol{u}_t + \boldsymbol{z}_0 u_z \text{: } = \gamma\boldsymbol{E}_t + \boldsymbol{z}_0 E_z \tag{9}$$

into a linear eigenvalue equation [5] Transversal parts and the longitudinal component of $\boldsymbol{u}$ are indicated by the subscripts t and z. An application of this transformation leads to a bilinear eigenvalue problem in γ^2 and β_0^2

$$\left[\mathcal{A} - \beta_0^2\mathcal{B} - \gamma^2\mathcal{C}\right]\boldsymbol{u} = \boldsymbol{0}. \tag{10}$$

The three matrix operators are given by

$$\mathcal{A} = \begin{bmatrix} \nabla_t \times \eta_{zz}[\nabla_t \times \boldsymbol{1}] & \boldsymbol{0} \\ \nabla_t \cdot \boldsymbol{\eta}_{tt} & \nabla_t \cdot \boldsymbol{\eta}_{tt}\nabla_t \end{bmatrix}$$

$$\mathcal{B} = \begin{bmatrix} \boldsymbol{\varepsilon}_{tt} & \boldsymbol{0} \\ \boldsymbol{0}^T & -\varepsilon_{zz} \end{bmatrix}$$

$$\mathcal{C} = \begin{bmatrix} \boldsymbol{\eta}_{tt} & \boldsymbol{\eta}_{tt}\nabla_t \\ \boldsymbol{0}^T & 0 \end{bmatrix}. \tag{11}$$

Nevertheless, a different transformation can be used [18] as follows:

$$\gamma \neq 0\text{: } \boldsymbol{u}_t + \boldsymbol{z}_0 u_z \text{: } = \boldsymbol{E}_t + \boldsymbol{z}_0\gamma E_z \tag{12}$$

which leads to a similar bilinear eigenvalue problem

$$\left[\mathcal{A}' - \beta_0^2\mathcal{B}' - \gamma^2\mathcal{C}'\right]\boldsymbol{u}' = \boldsymbol{0}. \tag{13}$$

$\boldsymbol{u}'$ is the solution and the new operators are given by

$$\mathcal{A}' = \begin{bmatrix} \nabla_t \times \boldsymbol{\eta}_{zz}[\nabla_t \times \boldsymbol{1}] & -\boldsymbol{\eta}_{tt}\nabla_t \\ \boldsymbol{0}^T & \nabla_t \cdot \boldsymbol{\eta}_{tt}\nabla_t \end{bmatrix}$$

$$\mathcal{B}' = \mathcal{B}$$

$$\mathcal{C}' = \begin{bmatrix} \boldsymbol{\eta}_{tt} & \boldsymbol{0} \\ -\nabla_t\boldsymbol{\eta}_{tt} & 0 \end{bmatrix}. \tag{14}$$

Relations and properties of both sets of operators will be discussed in Section II-B. For unique solutions of (10) and (13), the boundary conditions (3) are transformed via (9) and (12) to the following equations:

$$\boldsymbol{n}_0 \times \boldsymbol{u} = \boldsymbol{0}, \qquad \text{on } \partial\Omega_D \tag{15a}$$

$$\left.\begin{aligned} \nabla_t \times \boldsymbol{u}_t = 0 \\ \boldsymbol{n}_0 \cdot \boldsymbol{\eta}_{tt}[\boldsymbol{u}_t + \nabla_t u_z] = 0 \end{aligned}\right\}, \qquad \text{on } \partial\Omega_N \tag{15b}$$

$$\boldsymbol{n}_0 \times \boldsymbol{u}' = \boldsymbol{0}, \qquad \text{on } \partial\Omega_D \tag{16a}$$

$$\left.\begin{aligned} \nabla_t \times \boldsymbol{u}_t' = \boldsymbol{0} \\ \boldsymbol{n}_0 \cdot \boldsymbol{\eta}_{tt}\left[\gamma^2\boldsymbol{u}_t' + \nabla_t u_z'\right] = 0 \end{aligned}\right\}, \qquad \text{on } \partial\Omega_N. \tag{16b}$$

Here, $\partial\Omega_D$ and $\partial\Omega_N$ denote the boundaries to perfect electric conductors (PECs) and perfect magnetic conductors (PMCs).

B. Nonphysical Solution of the Vector Wave Equation

Before the application of any numerical method, the nonphysical solutions of the wave (2) and (8) will be indicated. These solutions exist because the set of (2) is only complete if $\beta_0 \neq 0$ is assumed. The source-freeness of the fields is not necessary guaranteed for $\beta_0 = 0$. Consequently, the enlargement of the solution space has already been done, considering (2) as a complete set of equations.

It is easy to prove that any function $\boldsymbol{E}_s$ that satisfies the boundary condition of Maxwell's equations given by

$$\beta_0 = 0\text{: } \boldsymbol{E}_s = \frac{1}{\gamma}\nabla_t\phi_s - \boldsymbol{z}_0\phi_s \tag{17}$$

is a solution of the problem with an unspecified source distribution.

Thus, for the different transformations (9) or (12), two different sets of nonphysical solutions end up from (17) as follows:

$$\beta_0 = 0\text{: } \boldsymbol{u}_s = \phi_s\boldsymbol{z}_0 - \nabla_t\phi_s \begin{cases} 1\text{: } \mathcal{A},\mathcal{B},\mathcal{C} \\ \frac{1}{\gamma^2}\text{: } \mathcal{A}',\mathcal{B}',\mathcal{C}'. \end{cases} \tag{18}$$

Each nonphysical solution is a solution of a linear eigenvalue problem, e.g.,

$$\beta_0 = 0\text{: } \left[\mathcal{A} - \gamma^2\mathcal{C}\right]\boldsymbol{u}_s = \boldsymbol{0} \tag{19}$$

because of

$$\mathcal{A}\boldsymbol{u}_s = \begin{bmatrix} \nabla_t \times \eta_{zz}\left[\nabla_t \times \nabla_t\phi_s\right] \\ \nabla_t \cdot \boldsymbol{\eta}_{tt}\nabla_t\phi_s - \nabla_t \cdot \boldsymbol{\eta}_{tt}\nabla_t\phi_s \end{bmatrix} = \boldsymbol{0}$$
$$\mathcal{C}\boldsymbol{u}_s = \begin{bmatrix} \boldsymbol{\eta}_{tt}\nabla_t\phi_s - \boldsymbol{\eta}_{tt}\nabla_t\phi_s \\ 0 \end{bmatrix} = \boldsymbol{0}.$$

Even for $\beta_0 \neq 0$, there are nonphysical solutions in the continuous problem, which depend on the set of matrix operators being used. These functions are solutions of the inverse eigenvalue problem, e.g.,

$$\left[\gamma^{-2}\left(\mathcal{A} - \beta_0^2\mathcal{B}\right) - \mathcal{C}\right]\boldsymbol{u}_s = \boldsymbol{0}. \tag{20}$$

For $\gamma \to \infty$, the possibility that a nonphysical solution occurs is related to the definiteness of the operator $\mathcal{C}$

$$\beta_0 \neq 0 \quad \gamma \to \infty\text{: } \mathcal{C}\boldsymbol{u}_s = \boldsymbol{0}. \tag{21}$$

In case of the operators (11), the additional nonphysical solutions $\boldsymbol{u}_s$ are given by

$$\beta_0 \neq 0 \quad \gamma \to \infty\text{: } \boldsymbol{u}_s = \boldsymbol{\nabla}_t\phi_s - \phi_s\boldsymbol{z}_0. \tag{22}$$

Likewise, for the set of operators from (14), additional nonphysical solutions $\boldsymbol{u}_s$ can be pointed out as follows:

$$\beta_0 \neq 0 \quad \gamma \to \infty\text{: } \boldsymbol{u}_s = \phi_s\boldsymbol{z}_0. \tag{23}$$

For $\beta_0 \neq 0$, both eigenvalue problems have nonphysical solutions at $\gamma \to \infty$. It is obvious that no special procedure is necessary for the numerical solution if we solve the eigenvalue equations at or close to $\gamma = 0$, [5], [12]. However, the price paid for are nonsymmetric operators, even for a simple example of an empty rectangular waveguide. Equation (8b) can be shifted to the operator $\mathcal{C}$ by multiplication with γ^2, which leads to quasi-symmetric matrix operators, e.g., [7], [14]. As a result, the new operator $\mathcal{A}$ become semidefinite and $\gamma = 0$ is an eigenvalue for both problems, which belongs to an infinite number of nonphysical solutions similar to (23). Therefore, convergence problems of the numerical computation of propagation constants close to $\gamma = 0$ are expected. Thus, numerical methods based on (10) and (13) are considered to be more promising.

C. Adjoint Operators and Bilinear Form

For the application of Galerkin's procedure, an inner product and a function space is defined.

$$\langle \boldsymbol{u}|\boldsymbol{v}\rangle\text{: } = \iint_\Omega \boldsymbol{u}^H\boldsymbol{v}\,\mathrm{d}\Omega, \quad \boldsymbol{u},\boldsymbol{v} \in {L_2}^3(\Omega) \tag{24}$$

$$U^{(2)} = \left\{\boldsymbol{u}|\boldsymbol{u} \in_2^3, \quad \nabla_t \times \nabla_t \times u_t \in L_2, \quad \nabla_t \cdot \nabla_t u_z \in L_2\right\}. \tag{25}$$

The function space $U^{(2)}$ assures well-defined operators. As usual, L_2 denotes the space of square integrable functions. Using these definitions, it is possible to write down a weak formula, also known as the equivalent wave equation. A solution is given by an element $\boldsymbol{u} \in U$, which satisfies the boundary conditions (15) and the equation

$$\forall\, \boldsymbol{v} \in U^{(2)}\text{: } \langle \boldsymbol{v}|\mathcal{A}\boldsymbol{u}\rangle - \beta_0^2\langle \boldsymbol{v}|\mathcal{B}\boldsymbol{u}\rangle - \gamma^2\langle \boldsymbol{v}|\mathcal{C}\boldsymbol{u}\rangle = 0. \tag{26}$$

The vector function $\boldsymbol{v}$ is called the test function, similar to the method of moments [19]. For further discussions, (26) is named the weak formula of the original problem. Integration by parts and the use of boundary conditions (15) to avoid partial derivations of second order leads to the bilinear form of (10).

$$F(\boldsymbol{v},\boldsymbol{u}) = A(\boldsymbol{v},\boldsymbol{u}) - \beta_0^2 B(\boldsymbol{v},\boldsymbol{u}) - \gamma^2 C(\boldsymbol{v},\boldsymbol{u}) = 0. \tag{27}$$

Its bilinear operators are given by

$$A(\boldsymbol{v},\boldsymbol{u}) = \left\langle \nabla_t \times \boldsymbol{v}_t|\eta_{zz}\nabla_t \times \boldsymbol{u}_t\right\rangle - \left\langle \nabla_t v_z|\eta_{tt}\left[\nabla_t u_z + \boldsymbol{u}_t\right]\right\rangle$$
$$B(\boldsymbol{v},\boldsymbol{u}) = \left\langle v_z|\varepsilon_{zz}u_z\right\rangle - \left\langle \boldsymbol{v}_t|\varepsilon_{tt}\boldsymbol{u}_t\right\rangle$$
$$C(\boldsymbol{v},\boldsymbol{u}) = \left\langle \boldsymbol{v}_t|\eta_{tt}\left[\nabla_t u_z + \boldsymbol{u}_t\right]\right\rangle.$$

In order to get a solution that satisfies the boundary conditions, it is sufficient to restrict the test functions and the solutions to be members of the functions space

$$U_D^{(1)} = \left\{\boldsymbol{u}|\boldsymbol{u} \in L_2^3, \quad \nabla_t \times u_t \in L_2^2, \quad \nabla_t u_z \in L_2^2, \quad \boldsymbol{z}_0 \times \boldsymbol{u} = \boldsymbol{0}, \quad \text{on } \partial\Omega_D\right\} \tag{28}$$

because the boundary condition (15b) is a natural condition of (27).

Now, an additional integration of the bilinear form (27) by parts and a renaming of the quantities ($\boldsymbol{u} \to \boldsymbol{v}$ and $\boldsymbol{v} \to \boldsymbol{u}^+$) leads to an equation, which defines the adjoint eigenvalue problem

$$\forall\, \boldsymbol{v} \in U^{(2)}\text{: } \langle \mathcal{A}^+\boldsymbol{u}^+|\boldsymbol{v}\rangle - \beta_0^2\langle \mathcal{B}^+\boldsymbol{u}^+|\boldsymbol{v}\rangle + \gamma^{*2}\langle \mathcal{C}^+\boldsymbol{u}^+|\boldsymbol{v}\rangle = 0 \Rightarrow \left[\mathcal{A}^+ - \beta_0^2\mathcal{B}^+ - \gamma^{*2}\mathcal{C}^+\right]\boldsymbol{u}^+ = \boldsymbol{0}. \tag{29}$$

The corresponding matrix differential operators are given by

$$\mathcal{A}^+ = \begin{bmatrix} \nabla_t \times \boldsymbol{\eta}_{zz}^H [\nabla_t \times \mathbf{1}] & -\boldsymbol{\eta}_{tt}^H \nabla_t \\ \mathbf{0}^T & \nabla_t \cdot \boldsymbol{\eta}_{tt}^H \nabla_t \end{bmatrix}$$
$$\mathcal{B}^+ = \begin{bmatrix} \boldsymbol{\varepsilon}_{tt}^H & \mathbf{0} \\ \mathbf{0}^T & -\varepsilon_{zz}^H \end{bmatrix}$$
$$\mathcal{C}^+ = \begin{bmatrix} \boldsymbol{\eta}_{tt}^H & \mathbf{0} \\ -\nabla_t \boldsymbol{\eta}_{tt}^H & 0 \end{bmatrix}. \tag{30}$$

During integration by parts, the following equations were used to suppress line integrals:

$$\boldsymbol{n}_0 \times \boldsymbol{u}^+ = \mathbf{0}, \qquad \text{on } \partial\Omega_D \tag{31a}$$
$$\left.\begin{aligned} \nabla_t \times \boldsymbol{u}_t^+ &= 0 \\ \boldsymbol{n}_0 \cdot \boldsymbol{\eta}_{tt}^H \left[\gamma^{*2} \boldsymbol{u}_t^+ + \nabla_t u_z^+\right] &= 0 \end{aligned}\right\}, \qquad \text{on } \partial\Omega_N. \tag{31b}$$

These equations are the boundary conditions of the adjoint problem. The adjoint matrix differential operators and boundary conditions are essentially the same as those from (14) and (16), however, all material quantities are complex conjugated and transposed. Therefore, the solution of the adjoint wave equation $\boldsymbol{u}^+$ is a solution, which belongs to a waveguide containing complex conjugated and transposed material tensors.

D. Simplifications for Symmetric Materials

In cases of simple materials, the adjoint solution $\boldsymbol{u}^+$ is strictly related to the original solution $\boldsymbol{u}$. To be unique in further discussions, $\boldsymbol{u}_\gamma$ denotes the solution of the original problem belonging to the eigenvalue γ, and $\boldsymbol{u}_{\gamma^*}^+$ is the adjoint solution belonging to the eigenvalue γ^*. However, the derivation of the adjoint wave equation implies the existence of a corresponding adjoint solution $\boldsymbol{u}_{\gamma^*}^+$ to $\boldsymbol{u}_\gamma$.

If a waveguide with symmetric, but complex media ($\boldsymbol{\varepsilon}_r = \boldsymbol{\varepsilon}_r^T$ and $\boldsymbol{\mu}_r = \boldsymbol{\mu}_r^T$) is supposed, the adjoint operators can be expressed by means of the original operators

$$\mathcal{A}^+ = \mathcal{A}^* \quad \mathcal{B}^+ = \mathcal{B}^* \quad \mathcal{C}^+ = \mathcal{C}^*.$$

Accordingly, it is possible to write down the adjoint solution in terms of the original solution

$$\begin{aligned} \left[\mathcal{A}^+ - \beta_0^2 \mathcal{B}^+ - \gamma^{*2} \mathcal{C}^+\right] \boldsymbol{u}_{\gamma^*}^+ &= 0 \\ \left[\mathcal{A} - \beta_0^2 \mathcal{B} - \gamma^2 \mathcal{C}\right] \boldsymbol{u}_{\gamma^*}^{+*} = 0 \Rightarrow \boldsymbol{u}_{\gamma^*}^+ &= \boldsymbol{u}_\gamma^*. \end{aligned} \tag{32}$$

Thus, it is sufficient to solve for one problem since the solution of the other is simply its complex conjugated counterpart.

In case of lossless media ($\boldsymbol{\varepsilon}_r = \boldsymbol{\varepsilon}_r^H$ and $\boldsymbol{\mu}_r = \boldsymbol{\mu}_r^H$), the operators are self-adjoint in the sense of the inner product

$$\mathcal{A}^+ = \mathcal{A} \quad \mathcal{B}^+ = \mathcal{B} \quad \mathcal{C}^+ = \mathcal{C}.$$

Considering the adjoint problem, the following relation appears:

$$\begin{aligned} \left[\mathcal{A}^+ - \beta_0^2 \mathcal{B}^+ - \gamma^{*2} \mathcal{C}^+\right] \boldsymbol{u}_{\gamma^*}^+ &= 0 \\ \left[\mathcal{A} - \beta_0^2 \mathcal{B} - \gamma^{*2} \mathcal{C}\right] \boldsymbol{u}_{\gamma^*}^{+*} = 0 \Rightarrow \boldsymbol{u}_{\gamma^*}^+ &= \boldsymbol{u}_{\gamma^*}. \end{aligned} \tag{33}$$

It can be concluded that a solution for the original problem with γ^* exist, if γ is a valid propagation constant. Starting from the original equation

$$\begin{aligned} \left[\mathcal{A} - \beta_0^2 \mathcal{B} - \gamma^2 \mathcal{C}\right] \boldsymbol{u}_\gamma &= 0 \\ \left[\mathcal{A}^+ - \beta_0^2 \mathcal{B}^+ - \gamma^2 \mathcal{C}^+\right] \boldsymbol{u}_\gamma = 0 \Rightarrow \boldsymbol{u}_\gamma^+ &= \boldsymbol{u}_\gamma \end{aligned} \tag{34}$$

shows that a solution always exist for the adjoint waveguide with an eigenvalue γ if γ^* is a valid propagation constant for the adjoint problem. In conclusion for lossless waveguides, for both problems, a pair of complex conjugate propagation constants (γ and γ^*) always exist. Real eigenvalues γ^2 are not guaranteed (see, e.g., Fig. 6). However, if γ^2 is real, the following relations occur [20]:

$$\boldsymbol{u}_{\gamma^*}^+ = \boldsymbol{u}_\gamma^+ = \boldsymbol{u}_\gamma = \boldsymbol{u}_{\gamma^*}. \tag{35}$$

E. Bi-Orthogonality Relations

For waveguides with nonsymmetric transversally anisotropic materials, the space of the original and adjoint solutions are both complete [20], but neither is a set of orthogonal functions. Together they form a set of bi-orthogonal functions, which will be shown in this section. To this end, the physical solutions of the original problem $\boldsymbol{u}_k$ with the propagation constant γ_k and the physical solutions of the adjoint problem $\boldsymbol{u}_{i^*}^+$ with γ_i^* as the propagation constant are considered. Due to the completeness of both spaces, they can be used mutually as test functions.

The adjoint and original solutions are taken from the same weak formula (26) and can be written as follows:

$$A(\boldsymbol{u}_{i^*}^+, \boldsymbol{u}_k) - \beta_0^2 B(\boldsymbol{u}_{i^*}^+, \boldsymbol{u}_k) = \gamma_k^2 C\left(\boldsymbol{u}_{i^*}^+, \boldsymbol{u}_k\right) = \gamma_i^2 C\left(\boldsymbol{u}_{i^*}^+, \boldsymbol{u}_k\right). \tag{36}$$

A subtraction of the left-hand sides results into the bi-orthogonality relation between the original and adjoint solution

$$\left(\gamma_k^2 - \gamma_i^2\right) C(\boldsymbol{u}_{i^*}^+, \boldsymbol{u}_k) = 0 \tag{37}$$

which can also be written in terms of the operator $\mathcal{C}$

$$\gamma_i^2 \neq \gamma_k^2 \text{:}\ C(\boldsymbol{u}_{i^*}^+, \boldsymbol{u}_k) = \langle \boldsymbol{u}_{i^*}^+ | \mathcal{C} \boldsymbol{u}_k \rangle = 0. \tag{38}$$

Using the definition of $\mathcal{C}$, a bi-orthogonality relation is obtained, which is close to the well-known power-like orthogonality relation [20]

$$\begin{aligned} \gamma_i^2 \neq \gamma_k^2 \text{:}\ \langle \boldsymbol{u}_{i^*}^+ | \mathcal{C} \boldsymbol{u}_k \rangle &= \iint_\Omega \boldsymbol{z}_0 \cdot \left[\boldsymbol{v}_{t,k} \times \boldsymbol{u}_{t,i^*}^{+*}\right] d\Omega = 0 \\ \boldsymbol{v}_{t,k} &= \boldsymbol{\eta}_{tt} \left[(\boldsymbol{u}_{t,k} + \nabla_t u_{z,k}) \times \boldsymbol{z}_0\right]. \end{aligned} \tag{39}$$

The vector function $\boldsymbol{v}_{t,k}$ represents a field, which is proportional to the magnetic field. Due to the squares in the propagation constants in (38), this relation does not distinguish between different propagation directions. The information about the propagation direction is shifted to the inverse transformation (9) or (12).

Now, the results from Section II-D can be used to obtain simpler forms of this equation. If waveguides with complex, but symmetric material tensors are considered, (32) can be used to point out an orthogonality relation in terms of the original solutions

$$\gamma_i^2 \neq \gamma_k^2 \colon \langle \boldsymbol{u}_{i^*} | \mathcal{C} \boldsymbol{u}_k \rangle = \iint_\Omega \boldsymbol{z}_0 \cdot [\boldsymbol{v}_{t,k} \times \boldsymbol{u}_{t,i}] \, d\Omega = 0 \quad (40)$$

or in terms of the adjoint solutions

$$\gamma_{i^*}^2 \neq \gamma_{k^*}^2 \colon \langle \boldsymbol{u}_{i^*}^{+*} | \mathcal{C} \boldsymbol{u}_{k^*}^{+} \rangle = \iint_\Omega \boldsymbol{z}_0 \cdot \left[\boldsymbol{v}_{t,k^*}^{+} \times \boldsymbol{u}_{t,i^*}^{+} \right] d\Omega = 0$$
$$\boldsymbol{v}_{t,k^*}^{+} = \boldsymbol{\eta}_{tt}^H \left[\left(\boldsymbol{u}_{t,k^*}^{+} + \nabla_t u_{z,k^*}^{+} \right) \times \boldsymbol{z}_0 \right]. \quad (41)$$

Therefore, both solutions are themselves orthogonal with respect to the time-varying power flow.

In case of lossless materials, relation (39) is simplified to

$$\gamma_i^2 \neq \gamma_k^2 \colon \langle \boldsymbol{u}_{i^*} | \mathcal{C} \boldsymbol{u}_k \rangle = \iint_\Omega \boldsymbol{z}_0 \cdot \left[\boldsymbol{v}_{t,k}^{*} \times \boldsymbol{u}_{t,i} \right] d\Omega = 0 \quad (42)$$

for the original and to

$$\gamma_i^2 \neq \gamma_k^2 \colon \langle \boldsymbol{u}_{i^*}^{+} | \mathcal{C} \boldsymbol{u}_k^{+} \rangle = \iint_\Omega \boldsymbol{z}_0 \cdot \left[\boldsymbol{v}_{t,k}^{+} \times \boldsymbol{u}_{t,i^*}^{+*} \right] d\Omega = 0$$
$$\boldsymbol{v}_{t,k}^{+} = \boldsymbol{\eta}_{tt}^H \left[\left(\boldsymbol{u}_{t,k}^{+} + \nabla_t u_{z,k}^{+} \right) \times \boldsymbol{z}_0 \right] \quad (43)$$

for the adjoint solutions. In other words, both sets are themselves orthogonal with respect to the time-averages power flow.

Although at the beginning of this section a restriction to physical solutions has been done, it is interesting to know what the role of the nonphysical solutions will be in this occasion. If (21) is considered, it can be seen that both sets of nonphysical solutions, i.e., original and adjoint, are orthogonal to all other solutions. Equation (39) becomes senseless for nonphysical solutions. Using these solutions as test functions, the following well-known equations appear:

$$\left\langle \boldsymbol{u}_s \right| \left[\mathcal{A}^+ - \beta_0^2 \mathcal{B}^+ - \gamma^{*2} \mathcal{B}^+ \right] \boldsymbol{u}^+ \rangle = 0$$
$$\Rightarrow \langle \phi_s | \nabla_t \cdot \boldsymbol{\varepsilon}_{tt}^H \boldsymbol{u}_t^+ - \varepsilon_{zz}^* u_z^+ \rangle = 0 \quad (44a)$$
$$\left\langle \boldsymbol{u}_s^+ \right| \left[\mathcal{A} - \beta_0^2 \mathcal{B} - \gamma^2 \mathcal{B} \right] \boldsymbol{u} \rangle = 0$$
$$\Rightarrow \langle \phi_s^+ | \nabla_t \cdot \boldsymbol{\varepsilon}_{tt} \boldsymbol{u}_t - \gamma^2 \varepsilon_{zz} u_z \rangle = 0. \quad (44b)$$

However, it is irony of fate that the nonphysical solutions guarantee the source freeness of the physical solutions in a weak sense. Note that this equation is also true if the solutions are expressed via basis functions, for which (18) remains valid. Obviously, for these basis functions, the so-called inclusion condition is only true if the dimension of the spanned function space is infinite [27], [28].

III. Applying the FEM

A. Matrix Eigenvalue Equation

Both weak formulations, i.e., original and adjoint, have the same bilinear form (27), which contains only partial derivations of first order. In order to solve (27) numerically, the function space $U_D^{(1)}$ is replaced by a subspace of finite dimension N

$$U_{D,N}^{(1)} = \text{Span}\,\{\boldsymbol{w}_1, \ldots, \boldsymbol{w}_N\} \subset U_D^{(1)}. \quad (45)$$

$\boldsymbol{w}_i$ is called a basis function. For the original and adjoint problem, the same function space is used (Galerkin's procedure) as follows:

$$\boldsymbol{u} \approx \mathbf{W}\boldsymbol{x} \quad \boldsymbol{u}^+ \approx \mathbf{W}\boldsymbol{x}^+ \quad \mathbf{W} = \{\boldsymbol{w_1}, \ldots, \boldsymbol{w_N}\}. \quad (46)$$

The vectors $\boldsymbol{x} = \{x_1, \ldots, x_N\}^T$ and $\boldsymbol{x}^+ = \{x_1^+, \ldots, x_N^+\}^T$ are the complex valued unknown degrees of freedom.

Inserting these approximations into the bilinear form (27)

$$\boldsymbol{x}^+, \boldsymbol{x} \in \mathbb{C}^N \colon F(\mathbf{W}\boldsymbol{x}^+, \mathbf{W}\boldsymbol{x}) = \mathbf{0}$$

and using the bilinearity of the operators allows withdrawing of the unknown vectors

$$\boldsymbol{x}^{+H} \left[\mathbf{A} - \beta_\mathbf{0}^\mathbf{2} \mathbf{B} - \gamma^\mathbf{2} \mathbf{C} \right] \boldsymbol{x} = 0. \quad (47)$$

Thus, the numerical solutions of the original and adjoint problem are simply the complex conjugated left and right eigenvectors of the linear eigenvalue equation (47). All matrices can be computed analytical as follows:

$$\mathbf{A} = A(\mathbf{W}, \mathbf{W}) \quad \mathbf{B} = B(\mathbf{W}, \mathbf{W}) \quad \mathbf{C} = C(\mathbf{W}, \mathbf{W}). \quad (48)$$

Note that the nonsymmetric operators A and C of (27) have lead to nonsymmetric matrices $\mathbf{A}$ and $\mathbf{C}$.

B. Approximation of Nonphysical Solutions

TCFEs have been successfully applied to suppress nonphysical solutions (see, e.g., [5]–[8]). However, explanations of how these TCFEs suppress these solutions are often limited to zero frequency and, thus, the spurious modes are often called the dc modes of the problem. In this section, the understanding of the occurrence of these nonphysical solutions will be improved via the deduction of a proper FE space $U_{D,N}^{(1)}$ from the bilinear form. It will be shown that the choice of basis functions is also important for the absence of the nonzero frequency spurious modes.

Let an approximation of a nonphysical solution be given by

$$\beta_0 \approx 0, \gamma \in \mathbb{C} \colon \tilde{\boldsymbol{u}}_s \approx [\nabla_t - \boldsymbol{z}_0] \phi_s \in U_{D,N}^{(1)}. \quad (49)$$

For this problem, the bilinear eigenvalue problem (27) is considered for an unchanged propagation constant $\gamma = 1$ with the eigenvalue β_0

$$\mathcal{A}(\tilde{\boldsymbol{u}}^+, \tilde{\boldsymbol{u}}_s) - \mathcal{C}(\tilde{\boldsymbol{u}}^+, \tilde{\boldsymbol{u}}_s) = \beta_0^2 \mathcal{B}(\tilde{\boldsymbol{u}}^+, \tilde{\boldsymbol{u}}_s). \quad (50)$$

In this equation, $\tilde{\boldsymbol{u}}^+ \in U_{D,N}^{(1)}$ is an approximation of the adjoint solution. Each linear combination of adjoint solutions is also an element of $U_{D,N}^{(1)}$. Therefore, a special function will be chosen as follows:

$$\tilde{\boldsymbol{u}}^+ = \tilde{\boldsymbol{u}}_{s,t} - \boldsymbol{z}_0 \tilde{u}_{s,z} \in U_{D,N}^{(1)}. \quad (51)$$

Using solutions of this type in (50) as test functions and assuming positive definite material tensors, the left-hand side of (50) can be written as

$$\begin{aligned} 0 \leq & \mathcal{A}(\tilde{\boldsymbol{u}}^+, \tilde{\boldsymbol{u}}_s) - \mathcal{C}(\tilde{\boldsymbol{u}}^+, \tilde{\boldsymbol{u}}_s) \\ = & \underbrace{\langle \nabla_t \tilde{u}_{s,z} + \tilde{\boldsymbol{u}}_{s,t} | \boldsymbol{\eta}_{tt} (\nabla_t \tilde{u}_{s,z} + \tilde{\boldsymbol{u}}_{s,t}) \rangle}_{\geq 0} \\ & + \underbrace{\langle \nabla_t \times \tilde{\boldsymbol{u}}_{s,t} | \eta_{zz} \nabla_t \times \tilde{\boldsymbol{u}}_{s,t} \rangle}_{\geq 0}. \end{aligned}$$

For this special case, $\beta_0 = 0$ can only be an eigenvalue if both terms vanish. Otherwise, the approximation of the nonphysical solution $\tilde{\boldsymbol{u}}_s$ will appear as a spurious solution with $\beta_0 > 0$. In order to shift this spurious solution back to $\beta_0 = 0$, a vector function space $U^{(1)}_{D,N}$ is needed, which is able to represent gradients of scalar functions in a pointwise sense over the whole waveguide domain Ω.

$$\begin{aligned} \nabla_t \times \tilde{\boldsymbol{u}}_s = & 0 \wedge \tilde{\boldsymbol{u}}_{t,s} = -\nabla_t u_{z,s} \\ \Rightarrow \tilde{\boldsymbol{u}}_s = & [\nabla_t - \boldsymbol{z}_0] \tilde{\phi}_s \in U^{(1)}_{D,N}. \end{aligned} \tag{52}$$

While doing this, the approximation of the nonphysical solution is moved to the approximation of the scalar function ϕ_s as follows:

$$\tilde{\boldsymbol{u}}_s \approx \boldsymbol{u}_s \rightarrow \tilde{\phi}_s \approx \phi_s. \tag{53}$$

Typically, in the FE approximation, $\tilde{\phi}_s$ is a member of a space of piecewise continuous polynomials of nth-order $P_n(\Omega)$. As noted, (15b) and (16b) are either natural boundary or natural continuity conditions. Thus, only (15a) and (16a) have to be ensured via the basis functions $\boldsymbol{w}_i$ at inner or outer boundaries. Consequently, these equations lead to tangential continuity of the transversal components and continuity of the z-components. Any further continuity restriction of the transversal components leads to an increased continuity condition of the z-component, e.g., the continuity of the normal component (for an isotropic, homogeneous waveguide) forces a continuously derivable z-component. As known from [8], this is not possible in an arbitrary FE mesh. Since the continuity of the normal component is assured via the bilinear form in a weak sense, all continuity conditions are taken into account [9].

However, (52) will also lead to a proper approximation of the other set of nonphysical solutions [see (22) and (23)]. The inner product of $\tilde{\boldsymbol{u}}_s$ with any possible function from $U^{(1)}_{D,N}$ vanishes identically.

$$\forall\, \tilde{\boldsymbol{u}}^+ \in U^{(1)}_{D,N}\colon \langle \tilde{\boldsymbol{u}}^+ | \mathcal{C} \tilde{\boldsymbol{u}}_s \rangle = C(\tilde{\boldsymbol{u}}^+, \tilde{\boldsymbol{u}}_s) = 0. \tag{54}$$

This is true vice versa for the adjoint nonphysical solution

$$\forall\, \tilde{\boldsymbol{u}} \in U^{(1)}_{D,N}\colon \langle \tilde{\boldsymbol{u}}_s^+ | \mathcal{C} \tilde{\boldsymbol{u}} \rangle = C(\tilde{\boldsymbol{u}}_s^+, \tilde{\boldsymbol{u}}) = 0. \tag{55}$$

Thus, (52) assures propagation constants $\gamma \rightarrow \infty$ for nonphysical solutions of the original and adjoint problem.

It is obvious that the relations for Section II-E will also be satisfied by the discretized problem. In [29], it has been discussed that, using covariant projection elements or edge elements, the physical solution will be orthogonal to all irrotational functions. This so-called inclusion condition has been proven in [21] to be sufficient, but not necessary. Neither the edge, nor covariant projection elements fulfill the inclusion condition. It can be seen from (44) that this condition is to strong with respect to the order of scalar polynomials.

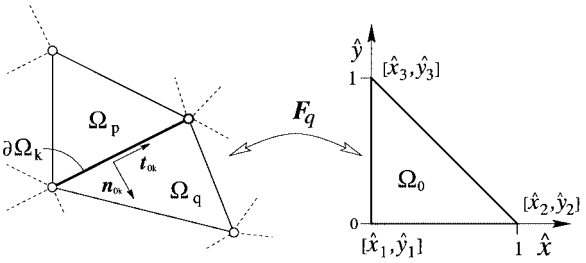

Fig. 2. Internal boundary and local transformation into master element Ω_0.

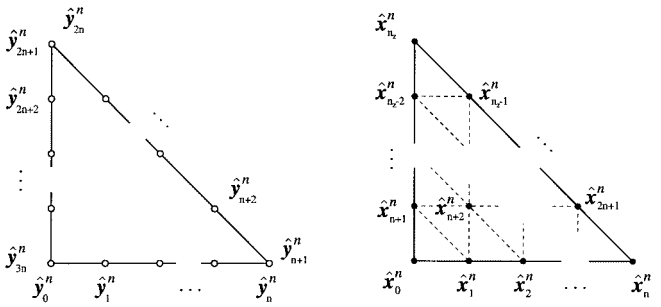

Fig. 3. Boundary and internal interpolation points.

C. FE Basis Functions of nth Order

For the FE approach, the waveguide domain is divided into a number of nonoverlapping triangles Ω_i as follows:

$$\Omega = \bigcup_{i=1}^{M} \Omega_i \wedge k \neq i\colon\ \Omega_k \cap \Omega_i = \{\emptyset\}. \tag{56}$$

Assuming tangential continuity between two FEs (see Fig. 3), the main focus in this section is the deduction of a polynomial basis for $\tilde{\boldsymbol{u}}$. Each Ω_i will be transformed into the master element Ω_0 via

$$\begin{aligned} \boldsymbol{x} = & \boldsymbol{F}_i(\hat{\boldsymbol{x}}) = \boldsymbol{M}_i \hat{\boldsymbol{x}} + \boldsymbol{b} \\ \hat{\boldsymbol{u}} = & \boldsymbol{M}_i^T \boldsymbol{u}(\boldsymbol{F}_i(\hat{\boldsymbol{x}})) \end{aligned} \tag{57}$$

$$\begin{aligned} \boldsymbol{x}_1^i = & \boldsymbol{F}_i(\boldsymbol{0}) \\ \boldsymbol{x}_2^i = & \boldsymbol{F}_i(\hat{\boldsymbol{x}}_0) \\ \boldsymbol{x}_3^i = & \boldsymbol{F}_i(\hat{\boldsymbol{y}}_0). \end{aligned} \tag{58}$$

Here, $\hat{\boldsymbol{u}}$ depicts the transformed vectorial function, $\boldsymbol{x}^T = [x, y]$ and $\hat{\boldsymbol{x}}^T = [\hat{x}, \hat{y}]$ are the vectors in the global and transformed system, the triangle points are given by $\boldsymbol{x}_q^i$, and $\hat{\boldsymbol{x}}_0$ and $\hat{\boldsymbol{y}}_0$ are the unit vectors in the $\hat{x}$ and $\hat{y}$ directions (see Fig. 2). Using these definitions, it can be shown that the curl always vanishes in both coordinate systems

$$\begin{aligned} \hat{\nabla}_t \times \hat{\boldsymbol{u}}_{s,t} = & \det M_i \nabla_t \times \tilde{\boldsymbol{u}}_{s,t} = 0 \\ \Leftrightarrow \hat{\boldsymbol{u}}_{s,t} = & \hat{\nabla}_t \hat{\phi}_s \wedge \hat{\phi}_s \sim \hat{u}_{s,z}. \end{aligned}$$

Therefore, all the following discussions are restricted to Ω_0. Furthermore, with the space of nth-order polynomials $P_n(\Omega_0)$,

(52) can be used to define an FE function space for $n \geq 1$ as follows:

$$U_n^s(\Omega_0) = \left\{ \hat{u}_{\hat{x},\hat{y}} \in P_{n-1}(\Omega_0), \hat{u}_z \in P_n(\Omega_0) \right\}. \tag{59}$$

Due to the tangential continuity, all gradients are approximated globally with an exact vanishing curl in Ω. To simplify the implementation of the FEM, it is useful to point out interpolation conditions in order to obtain global basis functions of $U_n^s(\Omega_0)$. Therefore, each local basis function is written as a linear combination of vector and scalar polynomials inside Ω_0 as follows:

$$\hat{\boldsymbol{w}}_{t,i} = \sum_{k=0}^{n-1} \sum_{l=0}^{k} \boldsymbol{c}_{i,kl} \hat{x}^{k-l} \hat{y}^l \quad \hat{w}_{z,i} = \sum_{k=0}^{n} \sum_{l=0}^{k} d_{i,kl} \hat{x}^{k-l} \hat{y}^l. \tag{60}$$

The $n_t = n(n+1)$ coefficient of the ith transversal local basis function $\boldsymbol{c}_{i,kl} \in \mathbb{C}^2$ and the $n_z = (n+1)(n+2)/2$ coefficients of the longitudinal local basis functions $d_{i,kl} \in \mathbb{C}$ are calculated by means of the following moments:

$$\boldsymbol{t}_0^k \cdot \hat{\boldsymbol{w}}_{t,i} \left(\hat{\boldsymbol{y}}_j^{n-1} \right)\big|_{\partial\Omega_0} = \delta_{ij}, \qquad \begin{cases} i \in [1, n_t] \\ j \in [1, 3n] \end{cases} \tag{61a}$$

$$\iint_{\Omega_0} \hat{\boldsymbol{q}}_j \cdot \hat{\boldsymbol{w}}_{t,i} d\Omega = \delta_{ij}, \qquad \begin{cases} i \in [1, n_t] \\ j \in [3n+1, n_t] \end{cases} \tag{61b}$$

$$\hat{w}_{z,i}(\hat{\boldsymbol{x}}_j^n) = \delta_{ij}, \qquad i, j \in \{1, n_z\}. \tag{61c}$$

$\hat{\boldsymbol{y}}_j^n$ denote the Lagrange interpolation points and the vectors $\boldsymbol{t}_0^k$ are the tangential vectors belonging to $3n$ different boundary interpolation points $\hat{\boldsymbol{x}}_j^{n-1}$ (see Fig. 3). The linear independent vector polynomials $\hat{\boldsymbol{q}}_j \in P_{n-2}^2$ are necessary to assure the linear independency of the FE basis functions. Previously, n_t linear matrix systems of $\mathbb{R}^{n_t \times n_t}$ and n_z linear matrix systems of $\mathbb{R}^{n_z \times n_z}$ have to be solved only once to calculate the unknown coefficients of the basis functions $\hat{\boldsymbol{w}}_{t,i}$ and $\hat{w}_{z,i}$. For $n \leq 2$ and $\Omega \in \mathbb{R}^2$, the moments (61) are those presented in [22] and [23]. Basis functions that span $U_n^s(\Omega_0)$ with $n = \{1, 2\}$ have already been used successfully in [10], [11], and [13].

Up to now, everything corresponds to an exact calculation of the propagation constants of the nonphysical solutions. Considering (52), one can see that n additional local basis functions $\hat{\boldsymbol{p}}_i^n$ exist, which are linear independent under the curl-operator

$$\frac{1}{2} \boldsymbol{z}_0 \cdot \hat{\boldsymbol{\nabla}}_t \times \hat{\boldsymbol{p}}_i^n = -\hat{y}^{n-i} \hat{x}^{i-1} \Rightarrow$$

$$U_n^h(\Omega_0) = \left\{ \hat{\boldsymbol{p}}_i^n = \begin{bmatrix} \hat{y}^{n-i+1} \hat{x}^{i-1} \\ -\hat{x}^i \hat{y}^{n-i} \end{bmatrix}, \qquad i \in \{1, \ldots, n\} \right\}. \tag{62}$$

Here, $U_n^h(\Omega_0)$ is the space of homogeneous vector polynomials of nth order. Note that these additional degrees of freedom will improve the approximation of the physical solutions, keeping the nonphysical solutions unchanged. With (62), (59) is completed to

$$U_n(\Omega_0) = U_n^s(\Omega_0) \oplus U_n^h(\Omega_0). \tag{63}$$

This space leads to complete polynomials of order $n-1$ in the space of the curl-operator for all three components. Since both FE spaces $U_n(\Omega_0)$ and $U_n^s(\Omega_0)$ deliver the same number of nonphysical solutions, a different rate of convergence is expected.

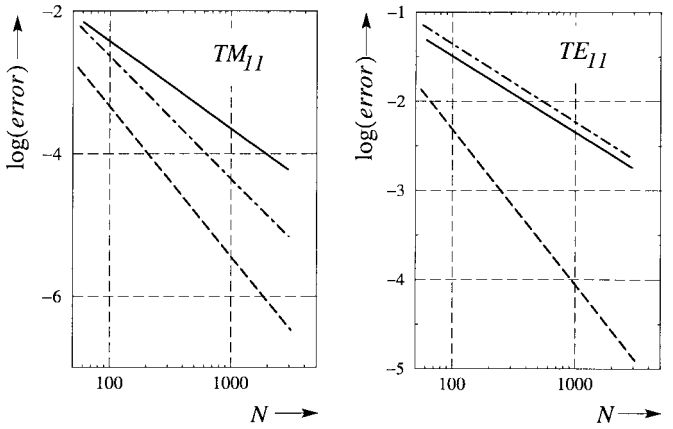

Fig. 4. Logarithm of the relative error (interpolated values) as a function of degrees of freedom N for the different FE spaces U_1 (——), U_2^s (- — -), and U_2 (- - -), empty rectangular waveguide with $a \times 2a$ at $\beta_0 a = 5$.

In order to obtain a set of local basis functions of $U_n(\Omega_0)$, the left-hand-side equation of (60) has been modified to

$$\hat{\boldsymbol{w}}_{t,i} = \sum_{k=0}^{n-1} \sum_{l=0}^{k} \boldsymbol{c}_{i,kl} \xi^{k-l} \eta^l + \sum_{k=1}^{n} h_{i,k} \hat{\boldsymbol{p}}_k^H. \tag{64}$$

Here, $h_{i,k} \in \mathbb{C}$ are the additional degrees of freedom, which increase the number of transversal unknowns in (61) to $n_t = n(n+2)$ (see [8]). Basis functions, which span $U_n(\Omega_0)$ with first and second order, have been used by many authors [5], [14], [24].

The incompleteness of $U_n^s(\Omega_0)$, however, leads to a unsatisfied rate of convergence, strongly depending on the considered problem. To show this, an empty rectangular waveguide with dimension $a \times 2a$ at the normalized frequency $\beta_0 a = 5$ has been considered. Fig. 4 contains the approximation error for the TE_{11} and TM_{11} modes for the first three FE function spaces.

For both modes (TE_{11} and TM_{11}), the rate of convergence for FEs spanning the spaces U_2 is always higher than those from U_1. In comparison, the rate of convergence of the U_2^s is different for TE_{11} and TM_{11} modes. Though elements with higher order have been used, the rate of convergence for the TE_{11} mode is even worse than the rate from U_1. The reason for this is the unsatisfied natural boundary condition of the bilinear form. This condition forces H_z to be continuous over the waveguide domain in a weak sense. However, this is only insufficiently possible because H_z is constant inside each Ω_i for U_2^s. Thus, for all kind of waveguide investigations with TE-like fields, the incomplete space U_n^s seems to be less attractive.

D. Numerical Solution of the Eigenvalue Problem

Usually, in the investigation of waveguide structures with the FEM, we are interested in some eigenvalues and eigenvectors $i \ll N$, close to a given complex number s at a given frequency. To speed up the computation time, the shifted and inverted problem is being solved as follows:

$$\tau \boldsymbol{x} = \boldsymbol{S}^{-1} \boldsymbol{C} \boldsymbol{x} \quad \tau^* \boldsymbol{x}^+ = \boldsymbol{S}^{-H} \boldsymbol{C}^H \boldsymbol{x}^+. \tag{65}$$

$\boldsymbol{S} = \boldsymbol{A} - \beta_0^2 \mathbf{B} - s\boldsymbol{C}$ denotes the shifted matrix, and $\gamma = \sqrt{\tau^{-1} + s}$ is the applied eigenvalue transformation.

The Lanczos algorithm from [5] has been proven to solve eigenvalue problems with symmetric operators efficiently. In the following, this algorithm is generalized to handle the nonsymmetric matrices of (47).

The basic idea of the Lanczos algorithm is the iterative construction of the matrices $\boldsymbol{Q}_i = [\boldsymbol{q}_1, \ldots, \boldsymbol{q}_i]$ and $\boldsymbol{Q}_i^+ = [\boldsymbol{q}_1^+, \ldots, \boldsymbol{q}_i^+]$, which transform the matrix $\boldsymbol{C}$ into a tridiagonal matrix $\boldsymbol{T}_i \in \mathbb{C}^{i\times i}$.

$$\boldsymbol{Q}_i^{+H} \boldsymbol{C} \boldsymbol{Q}_i = \boldsymbol{T}_i. \tag{66}$$

The column vectors $\boldsymbol{q}_k$ and $\boldsymbol{q}_k^+$ of $\boldsymbol{Q}_i$ and $\boldsymbol{Q}_i^+$ are assumed to be bi-orthogonal with respect to

$$1 \le k,l \le N\text{: } \boldsymbol{q}_k^{+H} \boldsymbol{S} \boldsymbol{q}_l = \delta_{kl}, \qquad \|\boldsymbol{q}_l\| = 1. \tag{67}$$

Consequently, the transformation (66) leads to ordinary eigenvalue systems of the original and adjoint problem of dimension $i \ll N$ as follows:

$$\begin{aligned} \tau \boldsymbol{y}_i &\approx \boldsymbol{T}_i \boldsymbol{y}_i \rightarrow \boldsymbol{x} \approx \boldsymbol{Q}_i \boldsymbol{y}_i \\ \tau^* \boldsymbol{y}_i^+ &\approx \boldsymbol{T}_i^H \boldsymbol{y}_i^+ \rightarrow \boldsymbol{x}^+ \approx \boldsymbol{Q}_i^+ \boldsymbol{y}_i^+. \end{aligned} \tag{68}$$

The tridiagonal structure of $\boldsymbol{T}_k$ allows an iterative process to calculate the new vectors $\boldsymbol{q}_{i+1}$ and $\boldsymbol{q}_{i+1}^+$ from the previous vectors $\boldsymbol{q}_i$ and $\boldsymbol{q}_i^+$ as follows:

$$t_{i+1,i} \boldsymbol{S} \boldsymbol{q}_{i+1} = \boldsymbol{C} \boldsymbol{q}_i - t_{i,i} \boldsymbol{S} \boldsymbol{q}_i - t_{i-1,i} \boldsymbol{S} \boldsymbol{q}_{i-1} \tag{69}$$

$$t_{i,i+1}^* \boldsymbol{S}^H \boldsymbol{q}_{i+1}^+ = \boldsymbol{C}^H \boldsymbol{q}_i^+ - t_{i,i}^* \boldsymbol{S}^H \boldsymbol{q}_i^+ - t_{i,i-1}^* \boldsymbol{S}^H \boldsymbol{q}_{i-1}^+. \tag{70}$$

These equations are solved via a sparse LU decomposition. Due to the decomposition, the solution of the transposed system and the new set of vectors $\boldsymbol{q}_{i+1}$ and $\boldsymbol{q}_{i+1}^+$ are obtained with no additional computation time after the first LU decomposition. A combinations of (67) with (69) and (70) define the coefficients of the tridiagonal matrix

$$t_{i,i} = \boldsymbol{q}_i^{+H} \boldsymbol{C} \boldsymbol{q}_i \quad t_{i,i+1} = \boldsymbol{q}_{i-1}^{+H} \boldsymbol{C} \boldsymbol{q}_i \quad t_{i+1,i} = \boldsymbol{q}_i^{+H} \boldsymbol{C} \boldsymbol{q}_{i-1}.$$

Each iteration leads to an enlargement of the matrix $\boldsymbol{T}_{i-1}$ to $\boldsymbol{T}_i$ with the entries $t_{i,i}$, $t_{i-1,i}$, and $t_{i,i-1}$.

The iteration is started with an arbitrary choice of initial vectors, e.g., $\boldsymbol{q}_1 = \boldsymbol{q}_1^+ = [1, \ldots, 1]^T / \sqrt{N}$. If $m+1$ solutions are desired, all new vectors $\boldsymbol{q}_i$ and $\boldsymbol{q}_i^+$ are bi-orthogonalized with the m previously calculated solutions

$$1 \le j \le m\text{: } \boldsymbol{q}_i^{+H} \boldsymbol{C} \boldsymbol{x}_j = 0 \quad \boldsymbol{q}_i^H \boldsymbol{C}^H \boldsymbol{x}_j^+ = 0. \tag{71}$$

Similar to [5], the relation $|y_i t_{i+1,i}| < e$ in the ith iteration step is checked for convergence. Here, y_i is the ith component of the eigenvector corresponding to the largest eigenvalue and e is the selected error tolerance.

IV. Numerical Results

In this section, numerical results of the presented method are compared with other methods. All presented results form the adjoint FEM are based on the function space U_2 so six nodal degrees of freedom for the z-component and eight degrees of freedom for the transversal components have been used.

A. Shielded Dielectric Image Line

The shielded dielectric image line of Fig. 5 is used to show the stability of the algorithm with respect to the occurrence of complex waves. Although all material parameters are lossless isotropic quantities, modes with complex propagation constant, called complex waves, exist [25]. These complex waves occur always in pairs with conjugated complex propagation constants. Fig. 6 shows the dependency of γ/β_0 on the normalized frequency $\beta_0 w$ for the first six modes. With growing frequency, a degeneration of a pair of complex waves to two hybrid modes EH_{21} and HE_{41} is observed, which is in excellent agreement with the results presented in [26]. No numerical instabilities have occurred during the calculation at cutoff $(\gamma = 0)$ because of (22) and (23). Note that the self-orthogonality of complex waves with respect to the average power is automatically handled because of the use of the corresponding adjoint solution [see (42)].

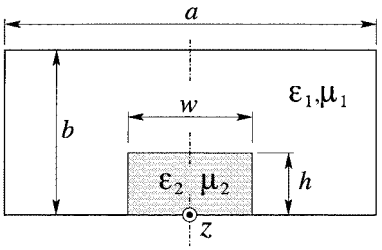

Fig. 5. Geometry of the shielded image waveguide.

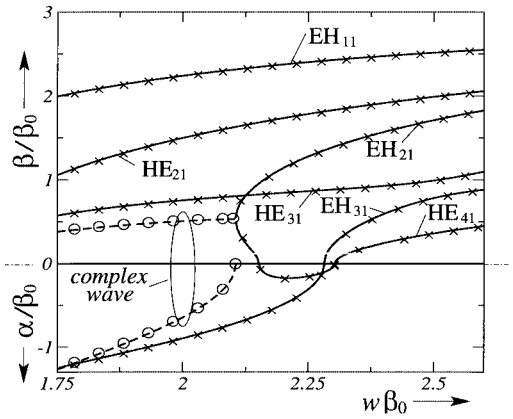

Fig. 6. Normalized propagation and normalized attenuation constants β/β_0 and α/β_0 of the first six hybrid modes for the waveguide shown in Fig. 5 as a function of normalized frequency $w\beta_0$. $a = 2b$, $b = 1.144783w$, $w = 2.15625h$, $\varepsilon_1 = \varepsilon_0$, $\varepsilon_2 = 9\varepsilon_0$, and $\mu_1 = \mu_2 = \mu_0$. —— and - - -: presented method, $\times$ and $\circ$: results from [26]. Degrees of freedoms are $N = 1500$.

B. Anisotropic Rectangular Waveguide

Next, the height of the dielectric image line will be increased to $h = b$. Both materials are assumed to have the same tensors so $\boldsymbol{\varepsilon}_1 = \boldsymbol{\varepsilon}_2 = \boldsymbol{\varepsilon}_r \varepsilon_0$

$$\boldsymbol{\varepsilon}_r = \begin{bmatrix} 18.59 - j2.57 & -3.88 + j1.03 & 0 \\ -3.88 + j1.03 & 14.1 - j1.39 & 0 \\ 0 & 0 & 11.86 - j0.8 \end{bmatrix} \tag{72}$$

Fig. 7 shows the normalized propagation and normalized attenuation constants β/β_0 and α/β_0 for the first two modes as functions of normalized frequency $w\beta_0$. Good agreement with the results presented in [13] is observed.

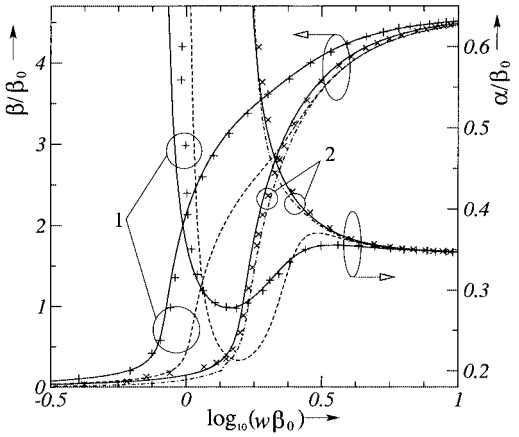

Fig. 7. Normalized propagation and normalized attenuation constants β/β_0 and α/β_0 for the first two modes as functions of the logarithm of the normalized frequency $w\beta_0$. ε_2 is defined by (72). Geometry parameters are: $b = 0.4454a$, $w = 0.2a$, and $h = b$. Results for homogeneous waveguide ($\varepsilon_1 = \varepsilon_2$ from (72), $\boldsymbol{\mu}_1 = \boldsymbol{\mu}_2 = \mu_0$): —— (presented method), $\times$, and $+$ (results from [13]). With added ferrite [$\varepsilon_2 = \varepsilon_0$ and $\boldsymbol{\mu}_2$ from (73)]: - - - and - — - (presented method). Degrees of freedom are: $N = 1700$.

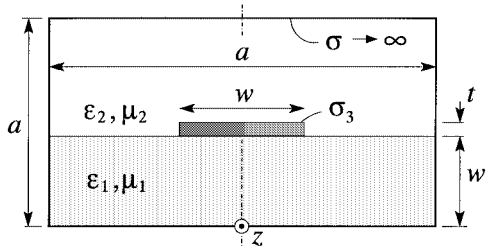

Fig. 8. Geometry of the anisotropic shielded microstrip line.

Furthermore, the center area was replaced by a ferrite with a permeability and permittivity given by

$$\boldsymbol{\mu}_2 = \begin{bmatrix} 0.875 & -j0.375 & 0 \\ j0.375 & 0.875 & 0 \\ 0 & 0 & 1 \end{bmatrix} \mu_0 \tag{73}$$

and $\varepsilon_2 = \varepsilon_0$, while the other materials are unchanged. A reduction of the normalized propagation constant can be observed for the fundamental mode, while the second mode is less affected. The symmetry of the materials is lost by adding this slab and the orthogonality relation is neither given by (40), nor (42). The need of the adjoint solutions for the algorithm showed in Section III-D is obvious.

C. Anisotropic Shielded Microstrip Line

The capability of the presented algorithm for microwave structures is shown by considering a shielded microstrip line with anisotropic materials (see Fig. 8). The permittivity of the substrate is given by

$$\boldsymbol{\varepsilon}_1 = \begin{bmatrix} \varepsilon_{xx} & \varepsilon_{xy} & 0 \\ \varepsilon_{xy} & \varepsilon_{yy} & 0 \\ 0 & 0 & \varepsilon_{zz} \end{bmatrix} (1 - j\tan\delta)$$

$$\begin{aligned} \varepsilon_{xx} &= \varepsilon_o \cos^2\theta + \varepsilon_e \sin^2\theta \\ \varepsilon_{xy} &= (\varepsilon_e - \varepsilon_o)\sin\theta\cos^2\theta \\ \varepsilon_{yy} &= \varepsilon_o \sin^2\theta + \varepsilon_e \cos^2\theta \\ \varepsilon_{zz} &= \varepsilon_o. \end{aligned}$$

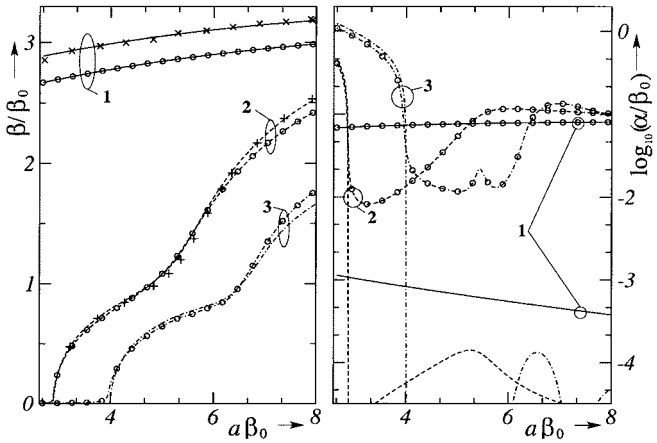

Fig. 9. Normalized propagation (β/β_0) and logarithm of normalized attenuation constants ($\log_{10}(\alpha/\beta_0)$) of the first three modes as a function of $a\beta_0$ for the waveguide shown in Fig. 8. Parameters are: $a = 10w$, $w = 25.4t$, $\varepsilon_e = 11.4\varepsilon_0$, $\varepsilon_o = 9.4\varepsilon_0$, $\boldsymbol{\mu}_2 = \mu_0$, and $\sigma_3 t Z_0 = 2.58 \cdot 10^5\pi$. Results for symmetric materials ($\theta = 0$, $\tan\delta = 0$, and $\boldsymbol{\mu}_2 = \mu_0$): ——, - - -, and - — - (presented method), $\times$, $+$ (results from [13]). Results for nonsymmetric materials [$\theta = \pi/4$, $\tan\delta = 0.05$, and $\boldsymbol{\mu}_2$ from (73)]: ⊖—⊖, ⊖- -⊖, and ⊖ — ⊖ (presented method). Degrees of freedom are: $N = 4200$.

Fig. 9 shows the normalized propagation and normalized attenuation constant of the first three modes as a function of $a\beta_0$ for two different materials. For a lossless anisotropic permittivity ($\theta = 0$, $\tan\delta = 0$) and vacuum permeability, the results of the adjoint FEM are in good agreement with those presented in [13]. In a further investigation, the crystal direction has been changed ($\theta = \pi/4$) and losses are added ($\tan\delta = 0.05$). The material above the substrate is replaced by a ferrite with a permeability tensor $\boldsymbol{\mu}_2$ given in (73). Thus, the symmetry of the materials is lost. The first mode is mostly affected by this modification (see Fig. 9).

V. Conclusions

An FEM has been presented, which is able to solve waveguides with nonsymmetric transversally anisotropic materials. Therefore, a generalized bilinear form has been deduced, which has been solved for the original and adjoint problem. Bi-orthogonality for the original and adjoint solution has been shown for general transversally anisotropic materials. All nonphysical solutions of the new bilinear form have been indicated analytically. The nonphysical solutions of the new bilinear form have: 1) an unspecified propagation constant for zero frequency or 2) a propagation constant at infinity for nonzero frequencies. It has been shown that the nonphysical solutions guarantee the absence of sources for the physical solutions in a weak sense. From the bilinear form, an nth-order FE function space has been derived, which explains the capability of all known tangential continuous vectorial FEs. All eigenvalues of the approximated nonphysical solutions are identical to their analytical counterparts.

For the numerical solution of the nonsymmetric algebraic eigenvalue problem, a Lanczos algorithm has been generalized to solve the original and adjoint problem with nearly no additional computation time. By means of simple, but critical examples, it has been shown that the method is suitable for the investigation of waveguide structures with arbitrary reflection-symmetric inhomogeneous material parameters, especially at or close to cutoff.

REFERENCES

[1] J. P. Webb, "Finite element analysis of dispersion in waveguides with sharp metal edges," *IEEE Trans. Microwave Theory Tech.*, vol. 36, pp. 1819–1824, Dec. 1988.

[2] W. Schroeder and I. Wolff, "A hybrid-mode boundary integral equation method for the normal- and superconducting transmission lines of arbitrary cross-section," *Int. J. Microwave Millimeter-Wave Computer-Aided Eng.*, vol. 2, pp. 314–330, Jan. 1992.

[3] D. R. Lynch and K. D. Paulsen, "Origin of vector parasites in numerical Maxwell solutions," *IEEE Trans. Microwave Theory Tech.*, vol. 39, pp. 383–394, Mar. 1991.

[4] Y. Lu and F. A. Fernandez, "An efficient finite element solution of inhomogeneous anisotropic and lossy dielectric waveguides," *IEEE Trans. Microwave Theory Tech.*, vol. 41, pp. 1215–1223, Mar. 1993.

[5] J. Lee, D. Sun, and Z. J. Cendes, "Full-wave analysis of dielectric waveguides using tangential vector finite elements," *IEEE Trans. Microwave Theory Tech.*, vol. 39, pp. 1262–1271, Aug. 1991.

[6] J. B. Davies, "Finite element analysis of waveguide cavities—a review," *IEEE Trans. Microwave Theory Tech.*, vol. 29, pp. 1578–1583, Mar. 1993.

[7] J. F. Lee, "Finite element analysis of lossy dielectric waveguides," *IEEE Trans. Microwave Theory Tech.*, vol. 42, pp. 1025–1031, June 1994.

[8] D. Sun, J. Manges, X. Yucan, and Z. Cendes, "Spurious modes in finite-element methods," *IEEE Antennas Propagat. Mag.*, vol. 37, pp. 12–24, Oct. 1995.

[9] J. P. Webb, "Edge elements and what they can do for you," *IEEE Trans. Magn.*, vol. 29, pp. 1460–1465, Mar. 1993.

[10] M. Koshiba, S. Maruyama, and K. Hirayama, "A vector finite element method with the high-order mixed-interpolation-type triangular elements for optical waveguiding problems," *IEEE Trans. Microwave Theory Tech.*, vol. 12, pp. 495–502, Mar. 1994.

[11] A. Shah, M. Koshiba, K. Hirayama, and Y. Hayashi, "Hybrid-mode analysis of multilayered and multiconductor transmission lines," *IEEE Trans. Microwave Theory Tech.*, vol. 45, pp. 205–211, Feb. 1997.

[12] S. V. Polstyanko, R. Dyczij-Edlinger, and J. F. Lee, "Fast frequency sweep technique for the efficient analysis of dielectric waveguides," *IEEE Trans. Microwave Theory Tech.*, vol. 45, pp. 1118–1125, July 1997.

[13] L. Nuño, J. Balbastre, and H. Castañé, "Analysis of general lossy inhomogeneous and anisotropic waveguides by the finite-element method (FEM) using edge elements," *IEEE Trans. Microwave Theory Tech.*, vol. 45, pp. 446–449, Mar. 1997.

[14] S. V. Polstyanko and J. Lee, "$H_1(\mathrm{curl})$ tangential vector finite element method for modeling anisotropic optical fibers," *J. Lightwave Technol.*, vol. 13, pp. 2290–2295, Nov. 1995.

[15] X. Q. Sheng and S. Xu, "An efficient high-order mixed-edge rectangular element method for lossy anisotropic dielectric waveguides," *IEEE Trans. Microwave Theory Tech.*, vol. 45, pp. 1009–1013, July 1997.

[16] K. S. Kundert, "Sparse matrix techniques," in *Circuit Analysis, Simulation and Design, Advances in CAD for VLSI*, A. Ruehli, Ed. Amsterdam, The Netherlands: Elsevier, 1986, vol. 3, pp. 281–324.

[17] A. F. Peterson, "Vector finite element formulation for scattering from two-dimensional heterogeneous bodies," *IEEE Antennas Propagat. Mag.*, vol. 43, pp. 357–365, Mar. 1994.

[18] J. Tan and G. Pan, "A new edge element analysis of dispersive waveguiding structures," *IEEE Trans. Microwave Theory Tech.*, vol. 43, pp. 2600–2607, Nov. 1995.

[19] R. F. Harrington, *Field Computation by the Moment Method*. New York: Macmillan, 1968.

[20] L. B. Felsen and N. Marcuvitz, *Radiation and Scattering of Waves*, ser. Electromagnetics Waves. Piscataway, NJ: IEEE Press, 1994.

[21] A. Caorsi, P. Fernandes, and M. Raffetto, "Toward a good characterization of spectrally correct finite element methods in electromagnetics," *Int. J. Comput. Math. Elect. Eng.*, vol. 15, pp. 21–35, May. 1996.

[22] J. C. Nedelec, "Mixed finite elements in R^3," in *Numerische Mathematik*. Berlin, Germany: Springer Verlag, 1980, vol. 35, pp. 315–341.

[23] F. Blanc-Castillo, M. Salazar-Palma, and L. E. García-Castillo, "Linear and second order edge-Lagrange finite elements for efficient analysis of wave-guide structures with curved contours," in *25th Eur. Microwave Conf.*, 1995, pp. 444–448.

[24] S. H. Wing and Z. J. Cendes, "Combined finite element-modal solution of three-dimensional eddy current problems," *IEEE Trans. Magn.*, vol. 24, pp. 2685–2687, Nov. 1988.

[25] A. Omar and K. Schuermann, "Complex and backward-waves modes in inhomogeneously and anisotropically filled wave guides," *IEEE Trans. Microwave Theory Tech.*, vol. MTT-35, pp. 268–275, Aug. 1987.

[26] J. Strube and F. Arndt, "Rigorous hybrid-mode analysis of the transition from rectangular waveguide to shielded dielectric image guide," *IEEE Trans. Microwave Theory Tech.*, vol. MTT-33, pp. 391–401, May 1985.

[27] S. Caorsi, P. Fernandes, and M. Raffetto, "Edge elements and the inclusion condition," *IEEE Microwave Guided Wave Lett.*, vol. 5, pp. 222–223, July 1995.

[28] ——, "Do covariant projection elements really satisfy the inclusion condition?," *IEEE Trans. Microwave Theory Tech.*, vol. 5, pp. 222–223, July 1995.

[29] C. W. Crowley, P. P. Silvester, and Hurwitz, Jr., "Covariant projection elements for 3D vector field problems," *IEEE Trans. Magn.*, vol. 24, pp. 397–400, Jan. 1988.

Volkmar Schulz was born in Minden, Germany, in 1968. He studied information processing at the University of Applied Science, Bielefeld, Germany, from 1989 to 1993. He received the Dipl.-Ing. and Dr.-Ing. degrees from the University of Paderborn, Paderborn, Germany, in 1996 and 2001, respectively.

He is currently with the Philips Research Laboratory of Hamburg, Hamburg, Germany, where his main focus is on high-frequency antennas, and two- and three-dimensional numerical methods.